Bulgarian Journal of Physics vol. **XX** (20XX) 1–10

Fano Resonance Characteristics and Modulation of Josephson Current in a T-shaped Double Quantum Dots Hybrid Nanojunction

Bhupendra Kumar
Department of Physics, Government Post Graduate College Dwarahat, 263653, Uttarakhand, India

Received *14 August 2026*

Abstract. We investigate the Fano resonance characteristics and their modulation in Josephson transport through a T-shaped double quantum dot system applying the Green's function approach in the framework of equation of motion technique. The Fano resonance in the Josephson current arises from interference between two distinct transport channels. We demonstrate that the Fano lineshapes can be tuned by varying the central dot's energy level and the interdot tunneling strength. Coulomb interaction enhances the asymmetry of the resonance and drives 0–π phase transitions. In particular, π-junction behavior emerges when the energy level of the central dot lies below the Fermi energy under strong interaction conditions.

KEY WORDS: Quantum dots, Fano resonance characteristics, Josephson junction.

1 Introduction

The Fano effect was first introduced by Ugo Fano in 1961 to describe the interference between discrete resonant states and a continuum of states [1]. This interference leads to a characteristic asymmetric resonance profile, often seen in the scattering of particles or the transmission spectra of quantum systems. In mesoscopic structures such as quantum dots, the Fano effect significantly influences the transport characteristics, including current–voltage behavior and conductance, by modifying the interference between different tunneling pathways. In a T-shaped double quantum dot (TDQD) configuration, electrons may either pass directly through the main quantum dot (QD_1) or or take an indirect route involving the side-coupled quantum dot (QD_2). The energy level of the QD_2 critically affects the Fano resonance, as it introduces a phase shift via elastic scattering that alters the interference pattern. When $\epsilon_{d2} = 0$, interference is

negligible, whereas for $\epsilon_{d2} \neq 0$ (or $\epsilon_{d2} < 0$) the phase shift approaches $\pi/2$ (or $-\pi/2$), respectively. This tunability allows both suppression and enhancement of transport through adjustments of the quantum dot energy levels and interdot coupling [2–4].

K. Osawa et al. [5] analyzed how Fano-type interference influences the dc Josephson current at zero temperature in a Josephson junction featuring two parallel transport channels. One channel corresponds to direct tunneling across an insulating barrier, while the other involves resonant transport mediated by a quantum dot. The Hartree–Fock framework is used to deal with the electron–electron interaction inside the quantum dot. The Kondo temperature is taken to be much smaller than the superconducting gap. The research shows that the Josephson critical current has an asymmetric resonance that depends on the energy level of the quantum dot. This behavior happens because the two tunneling processes in the system interfere with each other: one goes through the insulating barrier and the other goes through the resonant quantum dot. The research also finds that the critical current can change sign around the resonance point, which means that there is a $0 - \pi$ transition. The Fano interference and the Coulomb interaction in the QD work together to cause this change. These results indicate a Fano effect-induced $0 - \pi$ transition in double QD Josephson junctions, wherein the interference between direct and resonant tunneling is pivotal in regulating the I_{SC}, particularly in the presence of Coulomb interactions.

The current research examines the Fano resonance properties of the Josephson current, as well as the modulation of Fano line shapes resulting from fluctuations in quantum dot energy levels and Coulomb interactions within a system of DQD linked to two superconducting leads in a T-shaped arrangement. In this configuration, the QD_1 is directly linked to the leads, but QD_2 is solely connected to QD_1 and is isolated from the superconducting leads (see Fig. 1). We

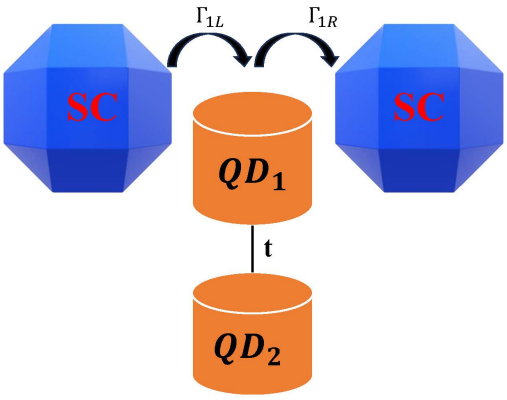


Figure 1. A schematic representation of a TDQD connected to BCS superconducting leads.

use the Green's equation of motion (EOM) technique [6,7] to look into the Fano characteristics in this T-shaped double quantum dot Josephson junction. In this model, the on-dot Coulomb interaction is considered solely on QD_1, while QD_2 is assumed to be non-interacting. QD_2 is modeled as a single non-interacting discrete level (δ-like localized state) with energy ϵ_{d2}, tunable via an external gate voltage. This level acts as a resonant scatterer, providing an additional interference path that gives rise to the characteristic asymmetric Fano-type line shapes in the Josephson current [2]. The analysis focuses on how interdot-tunneling affects the 0–π phase transition in the weak coupling regime, where the Coulomb interaction on QD_1 plays a decisive role. To maintain analytical simplicity, this interaction is confined to QD_1. It is well established that charge localization and many-body correlations in lateral quantum dots can strongly influence quantum interference phenomena such as the Fano effect and many-body effects like the Kondo resonance [8–13]. To address the Coulomb interaction on QD_1, we utilize the Hartree-Fock mean field approximation (HFA) [14–16]. While the HFA provides a qualitative description of quantum dot-based Josephson junction behavior, it becomes inadequate in the Kondo regime, where the Kondo temperature (T_k) surpasses the superconducting gap (Δ) [17]. Nonetheless, this limitation is confined to the strong coupling domain, whereas our investigation remains within the weak coupling limit [18], where the HFA remains valid and appropriate. This modeling approach is consistent with earlier theoretical studies of T-shaped double quantum dots [20,21] and with experimental realizations of double-dot Josephson devices [22–24].

2 Theoretical Formalism

We model the system using the Anderson impurity description of a DQD arranged in a T-shaped configuration and linked to two BCS superconducting electrodes. The total Hamiltonian of the system can be expressed as:

$$\hat{H} = \hat{H}_{leads} + \hat{H}_{QDs} + \hat{H}_{dot-lead} + \hat{H}_{interdot-tunneling} \tag{1}$$

where

$$\hat{H}_{leads} = \sum_{k\sigma,\alpha} \epsilon_{k\alpha} c^{\dagger}_{k\sigma,\alpha} c_{k\sigma,\alpha} - \left(\sum_{k\alpha} \Delta_{\alpha} c^{\dagger}_{k\uparrow,\alpha} c^{\dagger}_{-k\downarrow,\alpha} + h.c \right),$$

$$\hat{H}_{QDs} = \sum_{i=1}^{i=2} \sum_{\sigma} \epsilon_{di,\sigma} d^{\dagger}_{i\sigma} d_{i\sigma} + U_1 n_{1\sigma} n_{1\bar{\sigma}} \,,$$

$$\hat{H}_{dot-lead} = \sum_{k\sigma,\alpha} V_{k,\alpha} c^{\dagger}_{k\sigma,\alpha} d_{1\sigma} + h.c \,,$$

$$\hat{H}_{interdot-tunneling} = \sum_{\sigma} t(d^{\dagger}_{1\sigma} d_{2\sigma} + h.c) \,.$$

The Hamiltonian $\hat{H}_{\text{leads}}$ describes the superconducting leads, where $\alpha \in \{L, R\}$ indicates the left and right leads. The first part shows the free electrons in the superconducting leads. The creation and annihilation operators for electrons with spin σ, wave vector k, and energy $\epsilon_{k,\alpha}$ are $c^{\dagger}_{k\sigma,\alpha}$ and $c_{k\sigma,\alpha}$, respectively. The second part is the BCS Hamiltonian, which describes how Cooper pairs interact with each other.

The Hamiltonian of the DQD is denoted by $\hat{H}_{\text{dots}}$, with ϵ_{di} indicating the energy levels of the central quantum dot (QD_1) and QD_2, corresponding to the fermionic creation and annihilation operators $d^{\dagger}_{i\sigma}$ and $d_{i\sigma}$, respectively. U_1 represents the on-site Coulomb interaction at QD_1, and $n_{1\sigma} = d^{\dagger}_{1\sigma} d_{1\sigma}$ is the number operator that goes with it.

The term $\hat{H}_{dot-lead}$ refers to the tunneling Hamiltonian that connects the energy level of QD_1 to the superconducting leads. This is shown by the coupling strength $Vk\alpha$. Moreover, we have considered a symmetric coupling of QD_1 to both the left and right leads, i.e., $V_{1kL} = V_{1kR}$. The tunneling interaction between QD_1 and QD_2 is described by the final term, $\hat{H}_{interdot-tunneling}$, with a tunneling amplitude denoted by t.

The effective Hamiltonian yields from substituting the fermionic operators $c_{k\uparrow,\sigma}$ and $c^{\dagger}_{-k\downarrow,\sigma}$ with a Bogoliubov quasi-particle operator, is

$$
\begin{aligned}
\hat{H} = & \sum_{k\alpha} E_{k\alpha} (\beta^{\dagger}_{k\uparrow,\alpha} \beta_{k\uparrow,\alpha} + \beta^{\dagger}_{-k\downarrow,\alpha} \beta_{-k\downarrow,\alpha}) \\
& + \sum_{k\alpha} (V_{k\alpha} u^{*}_{k} \beta^{\dagger}_{k\uparrow,\alpha} d_{1\uparrow} + V_{k\alpha} u^{*}_{k} \beta^{\dagger}_{-k\downarrow,\alpha} d_{1\downarrow}) \\
& + \sum_{k\alpha} (V^{*}_{k\alpha} u_{k} d^{\dagger}_{1\uparrow} \beta_{k\uparrow,\alpha} + V^{*}_{k\alpha} u_{k} d^{\dagger}_{1\downarrow} \beta_{-k\downarrow,\alpha}) \\
& + \sum_{k\alpha} V_{k\alpha} v_{k} (\beta_{-k\downarrow,\alpha} d_{1\uparrow} - \beta_{k\uparrow,\alpha} d_{1\downarrow}) \\
& + \sum_{k\alpha} V^{*}_{k\alpha} v^{*}_{k} (d^{\dagger}_{1\uparrow} \beta^{\dagger}_{-k\downarrow,\alpha} - d^{\dagger}_{1\downarrow} \beta^{\dagger}_{k\uparrow,\alpha}) \\
& + \epsilon_{d_1} (d^{\dagger}_{1\uparrow} d_{1\uparrow} + d^{\dagger}_{1\downarrow} d_{1\downarrow}) + U_1 n_{1\sigma} n_{1\bar{\sigma}} \\
& + \epsilon_{d_2} (d^{\dagger}_{2\uparrow} d_{2\uparrow} + d^{\dagger}_{2\downarrow} d_{2\downarrow}) \\
& + t (d^{\dagger}_{1\uparrow} d_{2\uparrow} + d^{\dagger}_{1\downarrow} d_{2\downarrow} + d^{\dagger}_{2\uparrow} d_{1\uparrow} + d^{\dagger}_{2\downarrow} d_{1\downarrow})
\end{aligned} \tag{2}
$$

The formula $E_{k\alpha} = \sqrt{\epsilon^2{}_{k\alpha} + |\Delta_{\alpha}|^2}$ shows the energy of quasi-particle excitations in the superconducting leads. Coefficients u_k and v_k are expressed as

$$
|u_k|^2 = \frac{1}{2} \left(1 + \frac{\epsilon_{k,\alpha}}{\sqrt{\epsilon^2_{k,\alpha} + |\Delta_{\alpha}|^2}} \right), \tag{3}
$$

$$|v_k|^2 = \frac{1}{2}\left(1 - \frac{\epsilon_{k,\alpha}}{\sqrt{\epsilon_{k,\alpha}^2 + |\Delta_\alpha|^2}}\right). \tag{4}$$

We solve the effective Hamiltonian from Eq. (2) using the Green's function EOM method. To assess the phase- and temperature-induced transport properties of the T-shaped DQD Josephson junction, we compute the single-particle retarded Green's function of the QD_1, articulated in the Zubarev formalism [19].

$$\langle\langle d_\sigma(t); d_\sigma^\dagger(0)\rangle\rangle = -i\theta(t)\langle[d_\sigma(t), d_\sigma^\dagger(0)]_+\rangle\,.$$

The Fourier-transformed form of this single-particle retarded Green's function obeys the following EOM:

$$\omega\langle\langle d_\sigma|d_\sigma^\dagger\rangle\rangle_\omega = \langle\{d_\sigma, d_\sigma^\dagger\}_+\rangle + \langle\langle[d_\sigma, H]_-|d_\sigma^\dagger\rangle\rangle_\omega\,. \tag{5}$$

After solving the above effective Hamiltonian by using EOM method, the single particle retarded Green function of QD_1 with spin $\sigma =\uparrow$ can be expressed as:

$$\begin{aligned} G^r_{d\uparrow}(\omega) &= \langle\langle d_{1\uparrow}|d_{1\uparrow}^\dagger\rangle\rangle \\ &= \frac{\omega + E_{d1\downarrow} - \frac{t^2}{\omega+\epsilon_{d2}} - I_1}{(\omega + E_{d1\downarrow} - \frac{t^2}{\omega+\epsilon_{d2}} - I_1)(\omega - E_{d1\uparrow} - \frac{t^2}{\omega-\epsilon_{d2}} - I_2) - (I_3)^2}\,, \end{aligned} \tag{6}$$

where $E_{d1\uparrow} = \epsilon_{d_1} + U_1\langle n_{1\downarrow}\rangle$ and $E_{d1\downarrow} = \epsilon_{d_1} + U_1\langle n_{1\uparrow}\rangle$, and also

$$\begin{aligned} I_1 &= I_2 \\ &= -\sum_{\alpha\in L,R}\Big(\frac{\Gamma_\alpha\omega}{\sqrt{|\Delta_\alpha|^2-\omega^2}}\theta(\Delta_\alpha-|\omega|)+i(\frac{\Gamma_\alpha\omega}{\sqrt{\omega^2-|\Delta_\alpha|^2}}\theta(|\omega|-\Delta_\alpha)\Big), \end{aligned} \tag{7}$$

$$I_3 = -\sum_{\alpha\in L,R}\Big(\frac{\Gamma_\alpha\Delta_\alpha}{\sqrt{|\Delta_\alpha|^2-\omega^2}}\theta(\Delta_\alpha-|\omega|)+i(\frac{\Gamma_\alpha\Delta_\alpha}{\sqrt{\omega^2-|\Delta_\alpha|^2}}\theta(|\omega|-\Delta_\alpha)\Big). \tag{8}$$

I_1 and I_2 correspond to the diagonal elements of the self-energy, whereas I_3 represents the off-diagonal contribution arising from proximity-induced pairing due to the coupling between QD_1 and the superconducting leads. In this context, Γ_α denotes the coupling strength between the quantum dot and lead, and θ is the Heaviside step function.

To integrate the one-dot Coulomb interaction within QD_1, we utilize HFA. In this approach, the dot energy levels are renormalized as $E_{d_{1\sigma}} = \epsilon_{d_{1\sigma}} + U_1\langle n_{d_1\bar{\sigma}}\rangle$, where the occupancy of QD_1 is computed self-consistently using the following equation [25]:

$$\langle n_{d\sigma}\rangle = -\frac{1}{\pi}\int_{-\infty}^{\infty} f(\omega)Im(G_d^r(\omega))\,. \tag{9}$$

In the same way, the single particle retarded Green function of QD_1 with spin $\sigma =\downarrow$ can be expressed as:

$$G^r_{d\downarrow}(\omega) = \frac{\omega + E_{d1\uparrow} - \frac{t^2}{\omega+\epsilon_{d2}} - I_1}{(\omega + E_{d1\uparrow} - \frac{t^2}{\omega+\epsilon_{d2}} - I_1)(\omega - E_{d1\downarrow} - \frac{t^2}{\omega-\epsilon_{d2}} - I_2) - (I_3)^2}\,. \tag{10}$$

In a superconductor–quantum dot hybrid system, a significant contribution to the total transport originates from the Josephson current (I_{SC}), which is produced by the coherent tunneling of Cooper pairs between the superconducting electrodes. This current is phase-driven, depending explicitly on the superconducting phase difference $(\phi_L - \phi_R)$ across the leads. A comprehensive derivation of the phase-dependent Josephson current is provided in reference [26], and the final expression for the Josephson current can be found in [15, 26, 27].

Here, $f(\omega)$ is the Fermi-Dirac distribution function, Γ_α is the coupling strength between the QD_1 and the superconducting leads,Δ_α is the superconducting energy gap of the leads, and Δ_0 is the reference superconducting gap used for energy normalization (in section 3). $A(\omega)$ is the denominator of the single-particle retarded Green function given by 6 and 10 for spin $\uparrow$ and $\downarrow$, respectively. All quantities reported in section 3 are stated in units of Δ_0, which typically corresponds to a few meV

$$I_{SC} = \frac{e}{h}\sum_\sigma \int d\omega \frac{\Gamma^2_\alpha \Delta^2_\alpha}{\omega^2 - \Delta^2_\alpha} f(\omega) Im\left[\frac{-1}{A(\omega)}\right]. \tag{11}$$

3 Results and Discussion

In this section, we utilize the equations presented in the preceding section to calculate the Fano resonance characteristics of the Josephson current. For simplicity, we assume that both superconducting leads have the same superconducting energy gap, i.e., $\Delta_L = \Delta_R = \Delta$, and that the tunneling couplings between QD_1 and the superconducting leads are symmetric, so that $\Gamma_{1L} = \Gamma_{1R} = \Gamma$. The Coulomb interaction on QD_1 is represented by $U_1 = U$. Δ_0 is the reference superconducting gap used as the energy scale. All parameters in the numerical analysis are expressed in units of Δ_0 (in meV).

In this Figure 2, we explore the Fano resonance characteristics of the Josephson current (I_{SC}) as a function of the energy level of the QD_2 (ϵ_{d2}), with the QD_1 level fixed at $\epsilon_{d1} = 0.2\Delta_0$. At zero U, I_{SC} displays a typical asymmetric Fano lineshape with a pronounced dip around $\epsilon_{d2} = 0$, signifying destructive interference between two distinct transport pathways: one directly through the QD_1, which is linked to the superconducting leads, and the other indirectly through the QD_2. The Fano resonance arises due to quantum interference between a resonant bound state (localized in QD_2) and a continuum-like transport channel

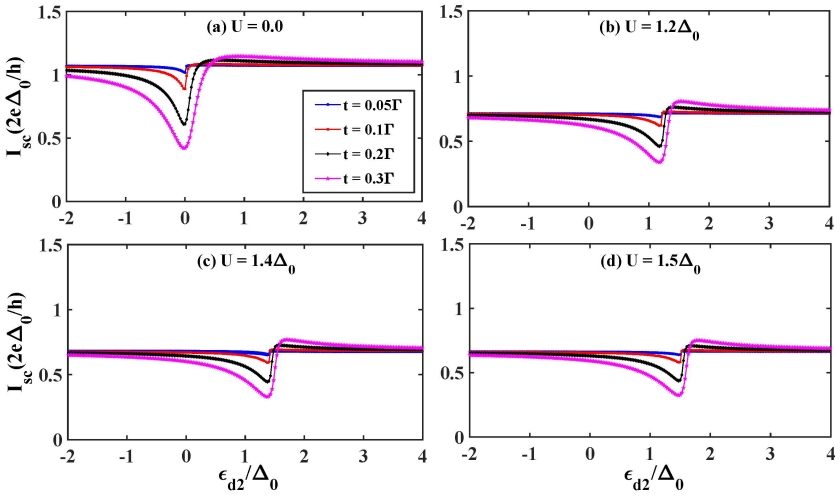


Figure 2. Josephson current plotted as a function of the energy level of QD_2 for various strengths of the interdot-tunneling and Coulomb interaction. The remaining parameters are fixed at $\epsilon_{d1} = 0.2\Delta_0$, $\Gamma = 0.5\Delta_0$.

via Andreev bound states in QD_1, leading to both interference and suppression (destruction) of supercurrent. As the interdot tunneling strength increases, the asymmetry of the Fano profile becomes more pronounced, and the destructive dip shifts and deepens, indicating stronger hybridization and enhanced interference effects. With the inclusion of U on QD_2, the asymmetry is further amplified due to correlation-induced modifications in the energy spectrum and tunneling pathways. Altogether, this interplay between tunneling, quantum interference, and electron correlations governs the emergence of Fano-type features in the Josephson current, revealing the coherent and phase-sensitive nature of transport in this T-shaped DQD Josephson junction.

We further demonstrate that the Fano lineshape of the Josephson current can be effectively tuned by adjusting the energy level of QD_1

In Figure 3, we plotted the modulation of Fano resonance features in the Josephson current (I_{SC}) as a function of the energy level of the QD_2 (ϵ_{d2}), for various values of the QD_1 energy level (ϵ_{d1}) and different strengths of the U. At zero U, the current exhibits a Fano-type valley centered at $\epsilon_{d2} = 0$, reflecting destructive interference between two transport channels: one through the directly coupled QD_1 and the other via the QD_2. The shape and position of the Fano lineshape are found to be highly sensitive to the value of ϵ_{d1}. As ϵ_{d1} is tuned, the peak of the Fano profile shifts from the positive ($\epsilon_{d2} > 0$) to the negative ($\epsilon_{d2} < 0$) side, indicating that the interference condition between the resonant and continuum-like channels is governed by the energy level alignment of QD_1.

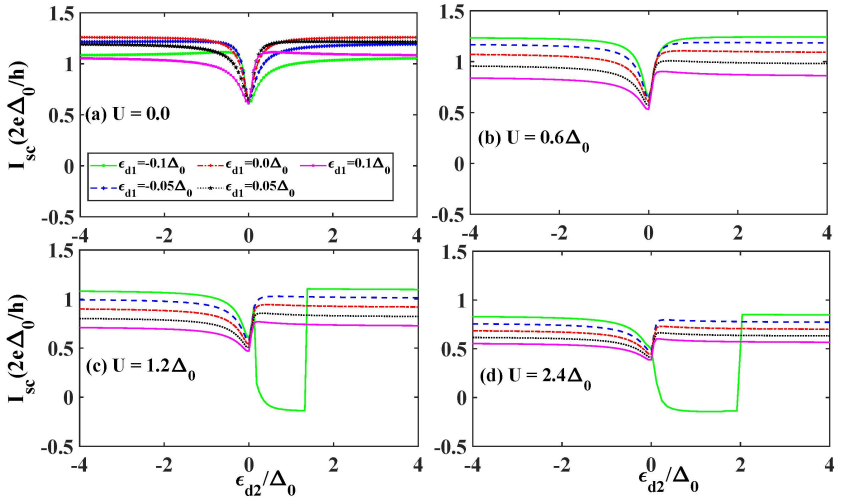


Figure 3. Josephson current versus ϵ_{d2} for different ϵ_{d1} and Coulomb interaction strengths. Other parameters are $t = 0.2\Delta_0$, $\Gamma = 0.5\Delta_0$.

Upon introducing a finite Coulomb interaction ($U = 0.6\Delta_0$), the Fano asymmetry becomes more pronounced due to correlation-induced modifications in the spectral properties of QD_2, although the system remains in the 0-junction state. At a moderate interaction strength ($U = 1.2\Delta_0$), a signature of a π-junction emerges specifically when $\epsilon_{d1} = -0.1\Delta_0$, i.e., when the energy level of QD_1 lies below the Fermi level. This transition to the π state results from a combined effect of Fano interference and electron-electron interactions that favor a ground state with a phase shift of π in the superconducting pairing. In contrast, when ϵ_{d1} is above the Fermi level, the system remains in the 0 state for the same U, demonstrating that ϵ_{d1} plays a decisive role in determining the junction phase. At a higher interaction strength ($U = 2.4\Delta_0$), a broad valley associated with the π state develops, followed by a transition back to the 0 state as ϵ_{d2} is further tuned, suggesting a reentrant 0–π behavior. These results demonstrate that the Fano lineshape and the 0–π phase of the Josephson current can be effectively tuned via the QD_1 energy level and electron correlations, providing a rich platform for controlling quantum interference and phase coherence in superconducting quantum dot systems.

In our manuscript, we restrict our analysis to the Fano resonance features of the Josephson current, which comes from the interference between two transport channels. Further, the π transition is facilitated by the interplay of the Fano effect and the Coulomb interaction within the QD. The findings detailed in the manuscript align with the prior investigation of the Fano effect in quantum dot-based Josephson junctions [5]. However, we do not provide a quantitative analysis of this effect because our attention in the present work is to examine

the Fano resonance characteristics and modulation of Josephson current due to interdot tunneing and QD_1 energy level. A detailed study of the Fano effect with superconducting leads can be done in our further research work.

4 Conclusion and Outlook

We have analyzed Fano resonance features in the Josephson current of a T-shaped DQD Josephson junction by using Green's function approach. The interference between two distinct transport channels gives rise to asymmetric Fano-type lineshapes in the current. We observe that tuning the energy level of QD_1 and the t can actively modulates the Fano profile, shifting its peak position and asymmetry. The inclusion of Coulomb interaction further amplifies the resonance asymmetry and enables 0–π phase transitions, particularly evident when the gate-controlled dot level lies below the Fermi level. This confirms that Fano interference, combined with electron correlation, crucially shapes the Josephson transport in hybrid quantum dot systems.

These insights into Fano resonance control could offer potential for developing gate-tunable superconducting devices, including phase transistors, quantum interferometers, and Andreev qubit implementations where interference effects can be precisely engineered. The ability to switch between 0 and π-junction regimes through gate tuning and Coulomb interaction suggests applications in quantum logic elements and phase-based sensor technologies [13].

Acknowledgments

The author, Bhupendra Kumar, would like to express his gratitude to Dr. D. C. Pant for providing the research facilities in the PG College Dwarahat, Uttarakhand, India.

References

[1] U. Fano (1961) *Phys. Rev.* **124** *1866.*

[2] S.-guang Cheng and Q.-feng Sun, *J. Phys.: Condens. Matter* **20**, *505202, (2008).*

[3] T. Tanamoto and Y. Nishi, *Phys. Rev. B* **76**, *155319, (2007).*

[4] R. Schuster, E. Buks, M. Heiblum, D. Mahalu, V. Umansky and H. Shtrikman, *Nature* **385**, *417–420, (1997).*

[5] K. Osawa, S. Kurihara, and N. Yokoshi, *Phys. Rev. B* **78**, *224508, (2008).*

[6] L. V. Keldysh, *Zh. Eksp. Theor. Fiz* **47**, *1515-1527, (1964).*
L. V. Keldysh, *Sov. Phys.-JETP* **20**, *1018-1026, (1965).*

[7] H. Haug and A.-P Jauho, *Quantum Kinetics in Transport and Optics of Semiconductors (Solid-State Sciences), Springer Berlin, Heidelberg,* **2nd edn.**, *(2008)*, Ch. 12, pp. 182.

[8] J. Barański and T. Domański, *Phys. Rev. B* **84**, *195424, (2011).*

[9] J. Barański and T. Domański, *Phys. Rev. B* **85**, *205451, (2012).*
[10] K. P. Wójcik and I. Weymann, *Phys. Rev. B* **97**, *235449, (2018).*
[11] J. Barański, T. Zienkiewicz, M. Barańska and K. J. Kapcia, *Sci Rep* **10**, *2881, (2020).*
[12] A. G. Inostroza, M. Pacheco, A. M. Calle, E. C. Siqueira and P. A. Orellana, *Sci Rep* **11**, *3941, (2021).*
[13] A. G. Inostroza, A. M. Calle, E. C. Siqueira, M. Pacheco and P. A. Orellana , *Eur. Phys. J. Plus* **139**, *790, (2024).*
[14] A. V. Rozhkov and D. P. Arovas, *Phys. Rev. Lett.* **82**, *2788, (1999).*
[15] Y. Kleeorin, Y. Meir, F. Giazotto and Y. Dubi , *Sci Rep* **6**, *35116, (2016).*
[16] A. Martín-Rodero and A. L. Yeyati, *J. Phys.: Condens. Matter* **24**, *385303, (2012).*
[17] M. Žonda, V. Pokorný, V. Janiš and T. Novotný, *Sci Rep* **5**, *8821, (2015).*
[18] T. Meng, S. Florens, and P. Simon, *Phys. Rev. B* **79**, *224521, (2009).*
[19] D. N. Zubarev, *Usp. Fiz. Nauk* **71**, *71-116, (1960).*
D. N. Zubarev, *Sov. Phys. Usp.* **3**, *320, (1960).*
[20] Y. Tanaka, N. Kawakami, and A. Oguri, *Phys. Rev. B* **78**, *035444, (2008).*
[21] A.M. Calle, M. Pacheco and P.A. Orellana, *Physics Letters A* **377**, *1474-1478, (2013).*
[22] J. C. E. Saldaña, A. Vekris, G. Steffensen, R. Žitko et al., *Phys. Rev. Lett.* **121**, *257701, (2018).*
[23] D. Bouman, R. J. J. van Gulik1, G. Steffensen, D. Pataki et al., *Phys. Rev. B* **102**, *220505(R), (2020).*
[24] R. Delagrange, R. Weil, A. Kasumov, M. Ferrier, H. Bouchiat1, and R. Deblock, *Phys. Rev. B* **93**, *195437, (2016).*
[25] B. Kumar, S. Verma and Ajay, *Physica E Low Dimens. Syst. Nanostruct.* **166**, *116142, (2025).*
[26] B. Kumar, S. Verma, and Ajay, *J. Supercon. Nov. Magn.* **36**, *831, (2023).*
[27] Y. Zhu, Q.-feng. Sun and T.-han Lin, *J. Phys.: Condens. Matter* **13**, *8783, (2001).*